Maximum stretched flame speeds of laminar premixed counter-flow flames at variable Lewis number

Sean D. Salusbury and Jeffrey M. Bergthorson

Department of Mechanical Engineering, McGill University
Montreal, QC, H3A 2K6, Canada
Phone: +1 514-398-2003
Fax: +1 514 398-7365
Email: sean.salusbury@mail.mcgill.ca

Abstract

This paper examines Lewis-number effects on stretched, laminar, premixed flames near extinction. It presents the experimental measurement of maximum stretched flame speed and extinction limit for the premixed laminar combustion of selected low, unity and high-Lewis number mixtures. Stretched, fuel-lean, laminar flames of methane with Le $\cong$ 1, propane with Le $>$ 1 and hydrogen with Le $\ll$ 1 are studied experimentally in a counter-flow flame configuration. Flow velocity is measured in these flames by particle tracking velocimetry. Results show that a maximum reference flame speed exists for mixtures with Le $\gtrsim$ 1 at lower flame-stretch values than the extinction stretch rate. In contrast, a continually-increasing reference flame speed is measured for Le $\ll$ 1 mixtures until extinction occurs when the flame is constrained by the stagnation point. Laminar flame results are also compared to numerical simulations employing a one-dimensional stagnation flame model. The chemical-kinetic models for each respective mixture capture the important trends of a maximum in $s_{\mathrm{u,ref}}$ ahead of the extinction stretch rate for methane and propane, and an increasing $s_{\mathrm{u,ref}}$ to extinction for hydrogen. These results are important to the investigation of the leading edge theory of premixed turbulent combustion, in which maximum stretched flamelet speed is a key parameter.

Keywords

reference flame speed; flame stretch, Lewis number; preferential diffusion; hydrogen; methane; propane; particle tracking velocimetry

1 Introduction

The effects of hydrodynamic stretch and curvature are highly important in premixed combustion; properties of both laminar and turbulent flames depend on a mixture's response to these phenomena. Both stretch and curvature have been studied extensively for laminar combustion [e.g., 1–3]. Much of the theory describing such flames is now textbook material [e.g., 4]; however, detailed experimental results of premixed stagnation flames – especially highly-stretched flames *below* the extinction limit – are scarce. While there is a wealth of computational and experimental work investigating increasing stretch and the extinction stretch rate [5–8], as well as the Markstein lengths [9–14] of premixed laminar flames, there are few, if any, measurements of the maximum stretched flame speed prior to extinction. This maximum stretched flame speed is important in the study of premixed turbulent combustion, as discussed below.

This is an

Premixed, laminar flames can be studied experimentally using the powerfully simple geometry of the counter-flow burner [15, 16]. This apparatus provides clear boundary conditions and a compact experimental zone that is ideal for performing detailed local measurements of laminar flames. In the constrained flow geometry of a counter-flow burner, stretch limits the laminar flame's reaction zone thickness and causes extinction for mixtures with Lewis numbers ($\mathrm{Le} = \alpha/\mathcal{D}$) near unity, where α is the thermal diffusivity and $\mathcal{D}$ is the mass diffusivity of the deficient reactant. For cases in which thermal diffusivity dominates ($\mathrm{Le} > 1$), maximum flame temperature falls below adiabatic flame temperature and decreases with increasing stretch due to heat losses to the unburned mixture, causing extinction at lower flame stretch. When $\mathrm{Le} \ll 1$, burning rates are enhanced by preferential molecular diffusion of the deficient reactant into the reaction zone, such that stretched

flame temperature and flame speed are greater than the adiabatic flame temperature and unstretched laminar flame speed of the bulk reactant mixture, respectively [1]. Extinction occurs in such cases only when the flow conditions force the reaction zone against the stagnation surface and its thickness, and the associated residence time available for chemical reactions, is thereby reduced by the imposed physical constraint. Counter-flow burners have also been used in many fundamental studies of turbulent flames [17–19], as well as more recent investigations of detailed turbulent flame properties [20–24].

Preferential diffusion effects have also been observed for turbulent flames and have been explained by the theory of leading points. The theory was first put forward in literature by [25], was expanded in [26] and has figured prominently in recent studies [27–30]. The theory of leading points regards the turbulent flame front as a collection of stretched and curved laminar flamelets [2], as do many theories of turbulent premixed flames. The leading points of the flamelet are located on the front that propagates farthest into the unburned reactants. These leading fronts, or leading edges, must be positively curved. The leading points theory argues that the flame speed of these leading edges controls the overall propagation speed of the turbulent flame. The maximum stretched flame speed, $s_{\mathrm{u,max}}$, of a laminar flame has been shown to be the maximum speed at which a turbulent flamelet will propagate [25, 26]. Since the leading edge is stretched and positively curved, the local burning rate at the leading point will increase for $\mathrm{Le} < 1$ [1]. An increase in burning rate will drive the flame to propagate further into the unburned reactants, further increasing the curvature and stretch experienced by this leading point. This process of increasing velocity is predicted to continue until the leading point reaches $s_{\mathrm{u,max}}$ [29].

Additionally, results from experimental laminar flames may also be of great utility to combustion kineticists. To validate kinetic models, results from laboratory experiments can be compared directly to results from simulations of the same experiment. This method, direct comprehensive comparison, represents a departure from the traditional method of measuring multiple quantities in order to derive one fundamental target for comparison, typically via extrapolation. Direct comprehensive comparison can provide

results of equal quality, while reducing experimental complexity and uncertainty [31, 32]. Direct comprehensive comparison is most successful when the experimental apparatus is designed to maximize the physical simplicity in the domain's geometry and minimize uncertainty in all necessary measurements. With careful design, a simple numerical model of the domain, typically one-dimensional, can be used, reducing computational cost. Many recent studies have employed this technique and have contributed key experimental data to the numerical modelling community [33–41].

In summary, the experimental results in this paper will (1) provide new measurements of highly-stretched premixed flames below the extinction limit, (2) assess the accuracy of chemical kinetic models across all stretch rates and (3) measure $s_{\mathrm{u,max}}$ and investigate the effect of preferential diffusion. These experimental velocity measurements will be performed on stretched lean methane (CH_4), propane (C_3H_8) and hydrogen (H_2) flames. The preferential diffusion effects measured in this paper for laminar flames will also inform the study of local instantaneous burning rates in premixed turbulent flamelets in future work. Recent studies have investigated the effect of stretch and preferential diffusion on turbulent flamelets [28–30, 42]; studying stretch behaviour of laminar flamelets will ultimately lead to an improved understanding of turbulent premixed combustion.

2 Experimental method

Experiments for this investigation are performed in a counter-flow burner. Identical premixed fuel and air mixtures are sent to the top and bottom nozzles of the burner. These mixtures flow through 60 mm diameter bronze plena and high contraction-ratio nozzles with exit diameter of 20 mm, corresponding to $A_{\mathrm{plenum}}/A_{\mathrm{nozzle}} = 9$. The inner contour of the high-contraction ratio nozzle is designed to accelerate the flow into a flat profile without generating turbulence. A laminar, axisymmetric velocity profile exiting the burner nozzle leads to a flat flame profile, which allows the system to be reasonably modelled as one-dimensional flow [15, 36, 43]. An annular flow of inert gas through the co-flow noz-

zles helps to stabilize the edges of the flames. The gaseous jets, with equal compositions, velocities and momenta, impinge upon one another between the two nozzle assemblies, separated by a distance of $L = 24\,\text{mm}$ in these experiments. The nozzles and stagnation plane are shown in Fig. 1.

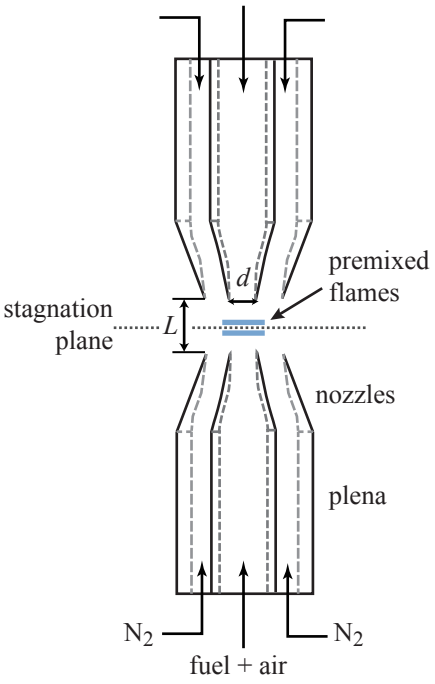

Figure 1: Schematic of nozzle assembly with premixed nozzles, inert coflow nozzles and plena.

For the experiments performed in this study, combustible mixtures are delivered to the burner assembly at room temperature. Each nozzle's flow rates of fuel and air are controlled by two mass flow controllers, each with an associated uncertainty of $\pm 0.9\%$ which leads to an uncertainty in the equivalence ratio, ϕ, of $\pm 1.3\%$. The gases are mixed in a 500 mL stainless steel mixing vessel filled with glass wool to promote mixing. From the mixing vessel, the mixture is seeded with micron-sized aluminum oxide particles for laser diagnostics.

The centreline flow velocity is measured using particle tracking velocimetry (PTV), performed by illuminating $1\,\mu$m alumina particles seeded into the flow with green laser

light, manipulated into a thin sheet [34, 44]. The laser used in these experiments is the Litron LDY 303, a high-repetition rate, frequency-doubled Nd:YLF laser. The laser emits 527 nm-wavelength light at 7.5 mJ per pulse at 1 kHz. The pulse frequency is selected to ensure that particles at the velocity minimum (in the flame zone) can be distinguished and varies between 800 Hz and 3.1 kHz.

The light scattered by the particles in the flow is captured by a Cooke PCO.2000, 2048×2048 pixel, 14-bit, monochrome CCD camera capable of capturing 14.7 images per second. To limit the interference of chemiluminescence in PTV images, a 527 nm optical notch filter is attached to the lens, a Nikon macro lens at f-stop = 5.8. Each exposure is set to last 50 ms to capture a streak of particles, as shown in Fig. 2. The spatial extent

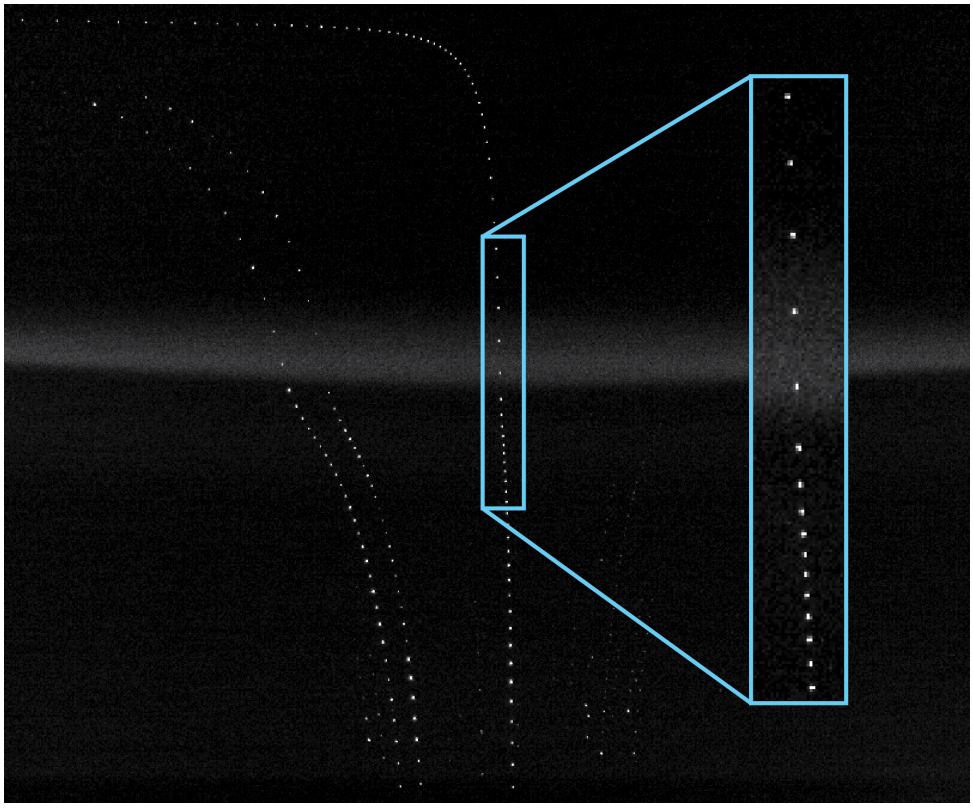

Figure 2: Raw PTV image from lower nozzle to stagnation plane with lean propane stagnation flame. Inset: Particle images used for fluid velocity computation.

of each image is approximately 36 mm $\times$ 36 mm with a resolution of 17.6 μm / pixel. At

least 30 particle streaks traveling on or near the centreline are processed by hand to give the velocity profiles for each run. An example resulting velocity profile is given in Fig. 3, where u is axial velocity and z is axial distance away from the stagnation plane. Note that this figure shows the results from all 30 processed streaks. The excellent overlap of each separate particle track illustrates the low uncertainty achievable by the PTV technique.

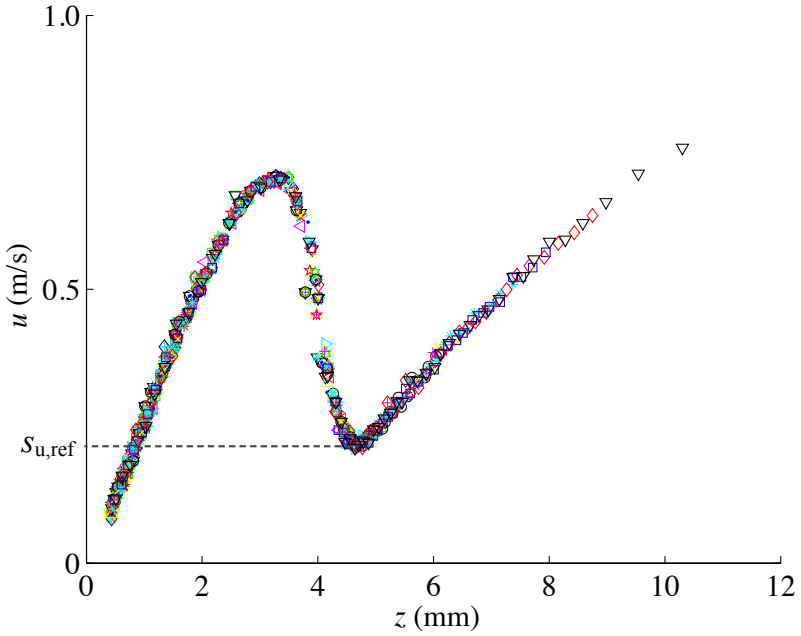

Figure 3: PTV velocity profile of propane-air flame at $\phi = 0.7$ with reference flame speed identified. Flow is from right to left, where $z = 0$ is the axial location of the stagnation plane.

This is an

For low and moderate stretch cases, the reference flame speed, $s_{u,ref}$, is the local minimum velocity upstream of the flame, as indicated in Fig. 3. The reference stagnation flame speed is measured from experimental data by fitting a second-order polynomial to the flow in the region of the reference point and computing the local minimum of the fit.

The propane-air velocity profile in Fig. 3 contains a well-defined local minimum, but the hydrogen-air profile in Fig. 4 does not. The low burning temperature of premixed hydrogen and air at $\phi = 0.19$ (in the range of $T_b = 1200\,\mathrm{K}$) results in no apparent increase in the particle velocity through the flame zone. For hydrogen-air flames, it is therefore necessary

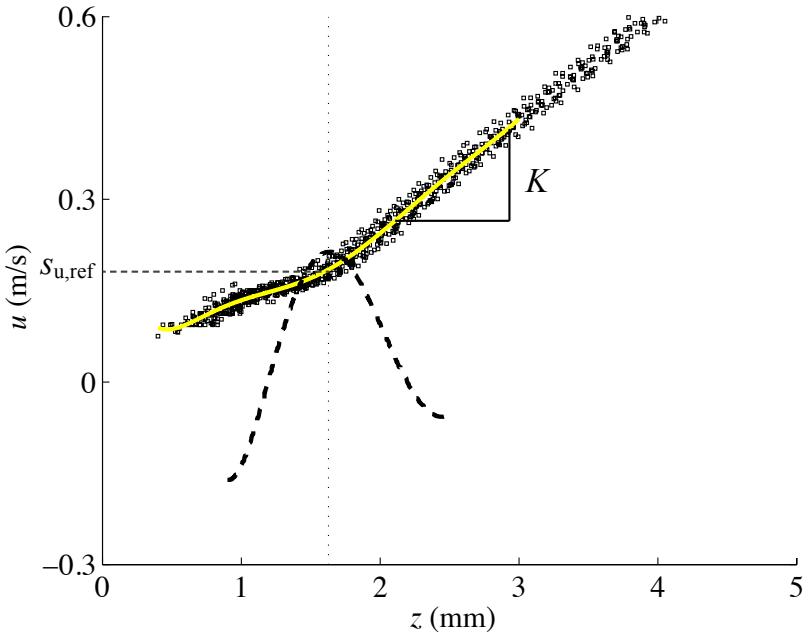

Figure 4: Reference flame speed determination for hydrogen-air velocity profile: PTV data (□), polynomial fit (solid), second derivative of polynomial (dash), reference z-location (dot).

This is an

to define an alternate method for determining a consistent $s_{u,ref}$ that is comparable to the $s_{u,ref}$ obtained from local minima, as in Fig. 3. The definition proposed here is:

$$s_{u,ref} = u|_{\max(u'')} \ . \tag{1}$$

This definition specifies $s_{u,ref}$ as the flow velocity where the second derivative of the flow profile with respect to z is a maximum, as shown in Fig. 4. The velocity determined by this definition is at the location of maximum change in the u-profile's slope, which indicates the transition from the unburned flow to the flame zone. Note that the point of local minimum in a velocity profile, used to determine $s_{u,ref}$ in flames with clear local minima, also satisfies the definition in Eqn. 1, which further justifies the proposed definition and will lead to consistent $s_{u,ref}$ measurements.

Lastly, the independent variable in these experiments, the flame stretch, is measured in the same way for all mixtures as the local stretch rate, K: the slope of a linear fit to the centreline flame profile at a position approximately 1.5 mm upstream of the reference flame speed position, where the velocity profile is approximately linear in z (see Fig. 4).

To model the flow, the following boundary conditions are specified: mixture composition, ambient pressure, temperature at the exit of the nozzle and velocity and stretch rate approximately 1.5 mm upstream of the flame. The mixture composition is set by mass flow controllers, temperature is measured by thermocouple at the nozzle exit. The velocity boundary conditions – inlet velocity and local stretch rate – are taken from the experimental PTV velocity profiles, which enables the one-dimensional model to capture the flame hydrodynamics [36].

3 Analytical and numerical models

This is an

Analytical model

In addition to experimental measurements of reference flame speed with stretch, two models, one analytical and one numerical, are employed in this study. First, experimental measurements of reference flame speed of stretched flames are compared to the analytical model of stretched laminar flame speed from [45]. This model predicts the effect of flame stretch on laminar flame speed as:

$$s_{\mathrm{L}} = s_{\mathrm{L}}^{\mathrm{o}} - \mathscr{L} K \tag{2}$$

where s_{L} is the stretched laminar flame speed, $s_{\mathrm{L}}^{\mathrm{o}}$ is the un-stretched laminar flame speed and K is the stretch rate. The Markstein length, $\mathscr{L}$, can be evaluated numerically with

$$\mathscr{L} = \frac{\alpha}{s_{\mathrm{L}}^{\mathrm{o}}}\beta \tag{3}$$

in which α is the thermal diffusivity and

$$\beta = \frac{\sigma \ln(\sigma)}{\sigma - 1} + \frac{\ell}{2} I_{\mathrm{o}} \tag{4}$$

where

$$\sigma = T_{\mathrm{b}}/T_{\mathrm{u}} \tag{5}$$

is the ratio of burned temperature, T_{b}, to unburned temperature, T_{u}, and

$$\ell = \frac{E_{\mathrm{a}} \cdot (\mathrm{Le} - 1)}{R T_{\mathrm{u}} \sigma^2}, \tag{6}$$

and

$$I_{\mathrm{o}} = \int_1^{\sigma} \frac{\ln s}{s - 1} \, \mathrm{d}s > 0 \tag{7}$$

where Le is the Lewis number of the mixture, E_{a} is the activation energy and R is the ideal gas constant.

This is an

Numerical model

To test the predictive accuracy of numerical models of one-dimensional premixed laminar flames, simulations of each experimental realization are conducted using the CHEMKIN-PRO software package [46]. Methane and air simulations use the GRI-Mech 3.0 mechanism [47], optimized for natural gas combustion with 53 species and 325 reactions. Propane and air flames are simulated by USC Mech II [48], designed for C1-C4 hydrocarbons, a mechanism with 111 species and 784 reactions. The updated Dryer H2-O2 mechanism with 13 species and 23 reactions is used for hydrogen and air flames [49].

CHEMKIN employs a one-dimensional, axisymmetric, steady-flow model to solve the impinging-jet flow [50]. This model has been shown to predict stagnation flame profiles accurately if the velocity boundary conditions are specified from experimental measurement, as shown in [34, 36, 40, 51–54].

To compare simulation results to experimental data, the following boundary conditions are measured and specified: chemical composition (set by mass flow controllers), pressure and temperature at the exit of both nozzles, as well as the velocity and stretch rate at the 'inlets' (approximately 1.5 mm upstream of the flames). Pressure in the simulations is assumed to be ambient atmospheric pressure, measured before each suite of runs. The temperature at the nozzle exit is measured by type K thermocouples that are removed before flames are lit. Velocity and stretch rate at the 'inlet' are determined by a parabolic fit to experimental data in the region upstream of the flame, as discussed in Section 2. The result of CHEMKIN's propane-air simulation using USC Mech II and these boundary conditions is shown in Fig. 5 for the full simulated z-range. The laminar, counter-flow flame is symmetrical across the $z = 0$ plane; therefore, experimental results shown in subsequent figures are only obtained for half of this domain.

This is an

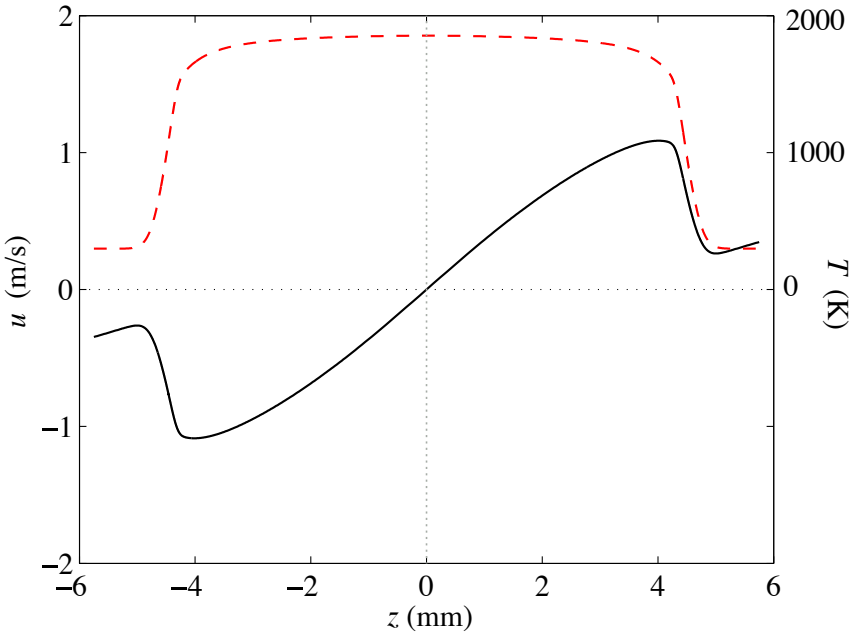

Figure 5: USC Mech II simulation of propane-air: u (solid), T (dash).

Convergence in numerical simulations is achieved at 2000 to 2500 grid points, GP, for CHEMKIN simulations. Figure 6 shows convergence curves for the three fuels and their associated chemical-kinetic models.

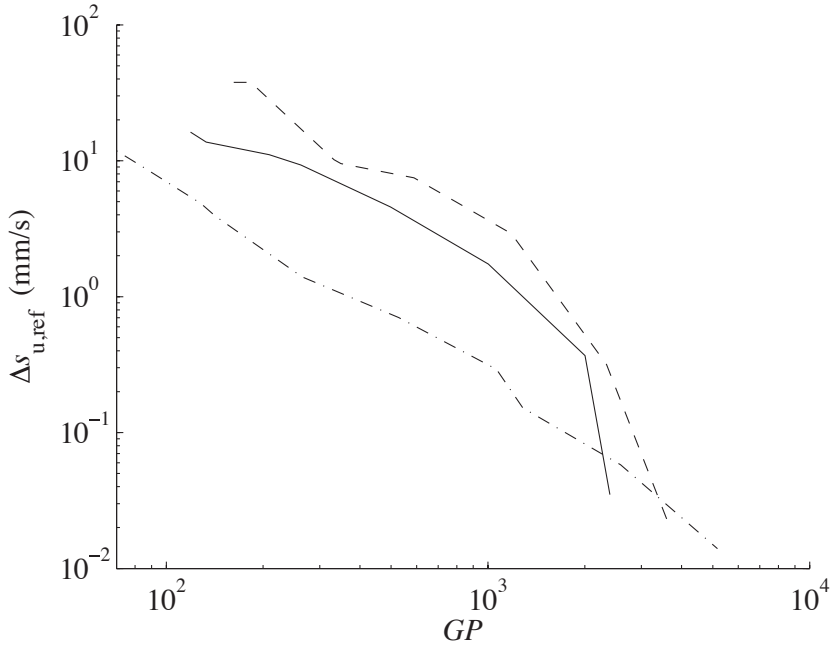

This is an

Figure 6: Convergence study of methane with GRI-Mech 3.0 (solid), propane with USC Mech II (dash) and hydrogen with Dryer H2 (dash dot).

With the numerical simulations converged, a final correction is applied to account for the effect of particle inertia and thermophoresis, which causes particle drift in the high-gradient regions of the flow [55–57]. The technique of particle motion correction used here is described in [57]. Thermophoretic corrections are performed assuming average particle size is as reported by the supplier, Noah Technologies, $d_\mathrm{p} = 1\,\mu$m. The most visible effect of this correction in the following stretched flame results is to decrease the peak of the simulated velocity profile, in the high-temperature region of the reaction zone. Comparison of both uncorrected GRI-Mech 3.0 simulation and the corrected particle motion curve is made in Fig. 7. The modelled particle motion captures the behaviour of the flow profile upstream of the flame (velocity increase) and downstream, towards the

This is an

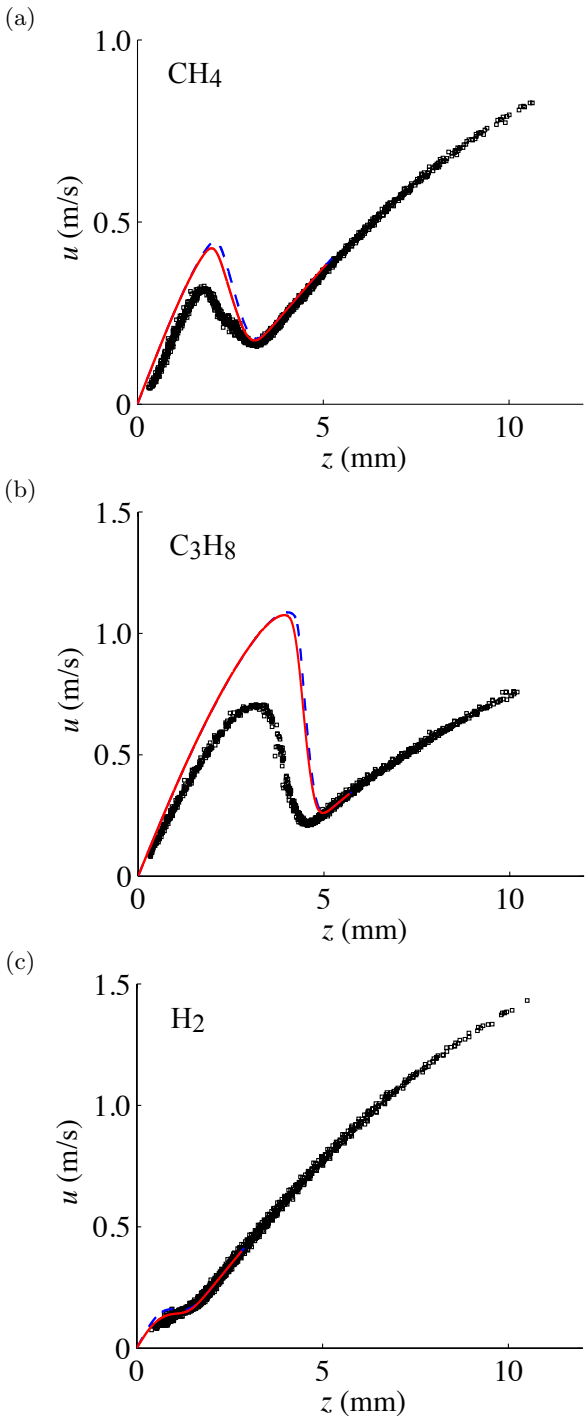

Figure 7: Flame profiles for (a) methane-air flame at $\phi = 0.6$ with local stretch rate $K = 113\,\mathrm{s}^{-1}$, (b) propane-air flame at $\phi = 0.7$ with local stretch rate $K = 123\,\mathrm{s}^{-1}$ and (c) hydrogen-air flame at $\phi = 0.19$ with local stretch rate $K = 187\,\mathrm{s}^{-1}$: PTV data (□), CHEMKIN simulation (dash), simulated particle motion (solid).

stagnation surface, but does not capture the irregular behaviour seen through the reaction zone. This experimental velocity profile for a stretched methane-air flame is representative of all profiles for that mixture. The temperature rise through the flame is expected to result in a smooth velocity rise, as seen in the propane-air profile in Fig. 3. Instead, the velocity profile contains a bump at approximately $z = 2\,\mathrm{mm}$. As shown in [55, 56], the particle motion through a stretched flame may lag behind the model for two principal reasons: (1) the true particle size is larger than expected, likely due to agglomeration, and (2) the effect of temperature gradients in the flame are not captured by the thermophoretic force estimation.

It is important to underscore, though, that while the modelled particle motion does not accurately capture the experimental particle motion through the peak velocity zone, particle motion modelling is not necessary in the upstream, $s_{\mathrm{u,ref}}$ and downstream regions. It is therefore sound to compare modelled $s_{\mathrm{u,ref}}$ to experimental results. The simulated reference flame speed values in Fig. 7 are in good agreement with experiment for methane and for hydrogen, with $s_{\mathrm{u,ref}}$ over-predicted for the propane flame.

This is an

4 Results and discussion

Table 1 lists the pertinent properties of lean, premixed methane-air, propane-air and hydrogen-air, the mixtures that are studied in this paper. Properties in Table 1 include unstretched laminar flame speed, $s_{\mathrm{L}}^{\mathrm{o}}$, as computed by free-flame simulations in Cantera [58]. Two calculated values are also shown in Table 1: Lewis number, as described above, and laminar flame thickness, δ_{L}, defined as:

$$\delta_{\mathrm{L}} = \frac{(\lambda/c_{\mathrm{p}})_{\circ}}{\rho_{\mathrm{u}} s_{\mathrm{L}}^{\mathrm{o}}} \ , \tag{8}$$

where $\lambda_{\circ}$ is the thermal conductivity at the inner layer temperature $T_{\circ}$, $c_{\mathrm{p},\circ}$ is specific heat at $T_{\circ}$, and ρ_{u} is density at the unburned reactants' temperature.

	CH_4 + Air $\phi = 0.6$	C_3H_8 + Air $\phi = 0.7$	H_2 + Air $\phi = 0.19$
s_L^o	11.5 cm/s	19.7 cm/s	8.75 cm/s
T_{ad}	1670 K	1860 K	1180 K
$T_\circ$	990 K	1080 K	740 K
ρ_u	1.14 kg/m^3	1.19 kg/m^3	1.09 kg/m^3
$\lambda_\circ$	74.5 mW/m·K	76.4 mW/m·K	64.5 mW/m·K
$c_{p,\circ}$	1260 J/kg·K	1300 J/kg·K	1170 J/kg·K
δ_L	0.450 mm	0.245 mm	0.580 mm
α	0.224 cm^2/s	0.209 cm^2/s	0.269 cm^2/s
$\mathcal{D}$	0.230 cm^2/s	0.112 cm^2/s	0.843 cm^2/s
Le	0.972	1.86	0.319

Table 1: Properties of mixtures used in stretched flame experiments.

Velocity results presented in this study are obtained using the counter-flow burner discussed in the previous section and are measured at the point of local velocity minimum ahead of the flame's reaction zone, the reference unburned velocity, $s_{u,ref}$, as illustrated in Fig. 8. At the reaction zone, this reference velocity is greater than the mixture's stretched

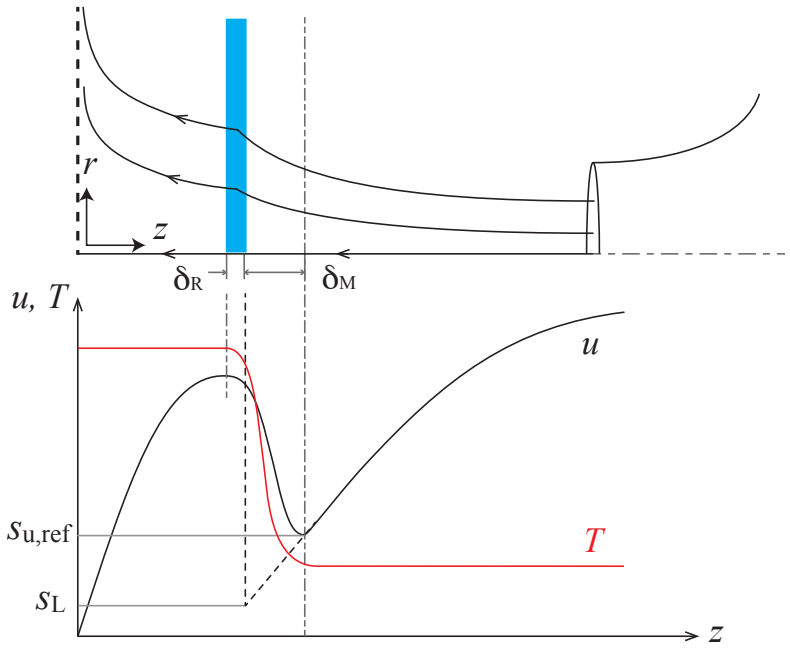

Figure 8: Schematic of the fluid velocity profile of an opposed flow flame, where δ_R is reaction zone thickness and δ_M is transport zone thickness.

laminar flame speed, s_{L}, as a consequence of the preheat zone [45]. The upstream edge of the flame experiences a temperature increase that brings about a rise in velocity before the reaction zone, or flame-sheet. The hydrodynamics of the laminar flame in stagnation flow is discussed thoroughly by Law [1] and in detail for this experimental geometry by Bergthorson *et al.* [36]. For mixtures with Le $\gtrsim 1$, s_{L} decreases with stretch since the rate of heat loss due to flame stretch exceeds the rate of chemical energy gain of the deficient reactant [1, 45]. As Fig. 9 illustrates for lean methane-air flames, $s_{\mathrm{u,ref}}$ increases as stretch rises from $K = 80\,\mathrm{s}^{-1}$ to $K = 148\,\mathrm{s}^{-1}$, even though s_{L} decreases with K, as shown in s_{L} predictions from the analytical model [45] in Fig. 10. As stretch increases, a steepening of the cold flow velocity profile just upstream of the reaction zone, coupled with the temperature profile across the flame, acts as a spatial filter of the velocity profile. This low-pass filter effect causes $s_{\mathrm{u,ref}}$ to increase even as s_{L} decreases [36]. However, near the extinction stretch rate, K_{ext}, reaction rates decrease so sharply that even the spatially-filtered $s_{\mathrm{u,ref}}$ value is seen to decrease. For this reason, stretched laminar methane flames exhibit a maximum stretched reference flame speed, $s_{\mathrm{u,max}}$, at a stretch rate below K_{ext}.

This is an

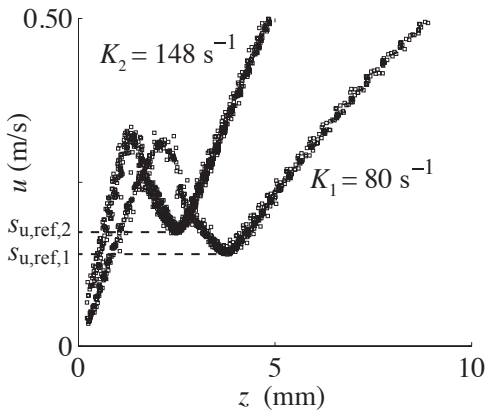

Figure 9: Particle tracking velocimetry measurements of methane-air at increasing stretch rate.

The reference flame speed and local stretch rate are extracted from each experimental run. It is then possible to plot $s_{\mathrm{u,ref}}$ at increasing K as in Fig. 10, in which the stretched laminar flame speed for each mixture is also shown as predicted by Tien's model [45].

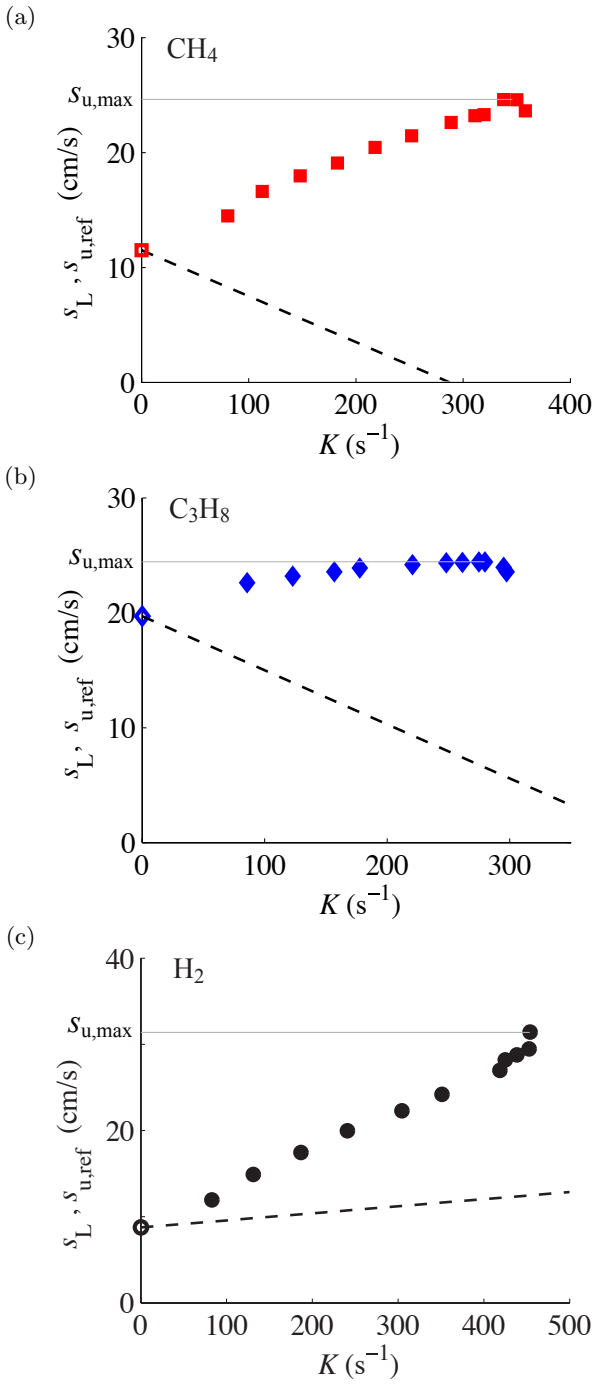

Figure 10: Reference flame speed, $s_{\mathrm{u,ref}}$ (closed symbols), simulated laminar flame speed (open symbols) and modelled stretched laminar flame speed, s_{L} (dashed lines) versus stretch for premixed counter-flow flames of (a) methane-air, (b) propane-air and (c) hydrogen-air.

These figures show the range of $s_{\mathrm{u,ref}}$, K and the distinct behaviour of each fuel. The range of velocities in Fig. 10a and Fig. 10c are comparable: both are measured near their respective $s_{\mathrm{L}}^{\mathrm{o}}$ at low K and climb with stretch. The increasing $s_{\mathrm{u,ref}}$ with K for methane-air shows that the filtering effect does indeed result in a marked increase in $s_{\mathrm{u,ref}}$ even with a moderate reduction in reaction rate. Similarly for hydrogen-air, the filtering effect results in a pronounced increase in $s_{\mathrm{u,ref}}$ as stretch rates, and the resulting s_{L} values, increase. In the case of the propane-air mixture, the decrease in s_{L} with K is so pronounced that the result is a comparatively flat $s_{\mathrm{u,ref}}$ profile with K. In these cases, Fig. 10 illustrates the divergence between $s_{\mathrm{u,ref}}$ experimental results (generally increasing with stretch) and modelled s_{L} (decreasing with stretch for methane and propane).

The extinction stretch rate, K_{ext}, for each mixture follows the trends predicted by theory: mixtures with $\mathrm{Le} \gtrsim 1$ extinguish by reduced reaction rates as stretch increases. The mixture with $\mathrm{Le} \ll 1$ is observed to extinguish with counter-flow flames at the stagnation surface; therefore extinction occurs due to flow constraint since reaction rates increase with K for the low Lewis number case. In order of increasing K_{ext}, the propane-air mixture with $\mathrm{Le} = 1.86$ is extinguished at $K = 297\,\mathrm{s}^{-1}$, methane and air with Le near unity is extinguished at $K = 358\,\mathrm{s}^{-1}$ and hydrogen-air with $\mathrm{Le} = 0.32$ is extinguished at $K = 454\,\mathrm{s}^{-1}$.

Reference flame speed near extinction leads to the key finding in these experiments. As predicted, the maximum $s_{\mathrm{u,ref}}$ is found at K below K_{ext} for methane-air and propane-air mixtures. For methane and air, $s_{\mathrm{u,max}}$ is measured as 24.6 cm/s at a stretch rate of $K = 338\,\mathrm{s}^{-1}$, approximately $20\,\mathrm{s}^{-1}$ below K_{ext} for that mixture. Additionally, methane-air results show only a moderate decrease in $s_{\mathrm{u,ref}}$ between its maximum and extinction. The maximum $s_{\mathrm{u,ref}}$ for propane and air occurs at a similar distance from its extinction stretch rate: $s_{\mathrm{u,max}} = 24.4\,\mathrm{cm/s}$ is measured at $K = 262\,\mathrm{s}^{-1}$. In the propane-air case, however, the flame speed near extinction begins to decrease considerably, relative to the range of $s_{\mathrm{u,ref}}$. In the final case of hydrogen-air, there is no decrease in $s_{\mathrm{u,ref}}$ near K_{ext}. The reaction rate in these flames continues to increase, the flame continues to move toward

the stagnation surface; consequently, the maximum reference flame speed is measured at the extinction stretch rate as $s_{\mathrm{u,max}} = 31.4\,\mathrm{cm/s}$.

To compare the reference flame speeds and extinction stretch rates directly, it is instructive to plot results for the three mixtures together, as in Fig. 11, in which $s_{\mathrm{u,ref}}$ is normalized by the respective laminar flame speed, $s_{\mathrm{L}}^{\mathrm{o}}$, of that mixture. The small range

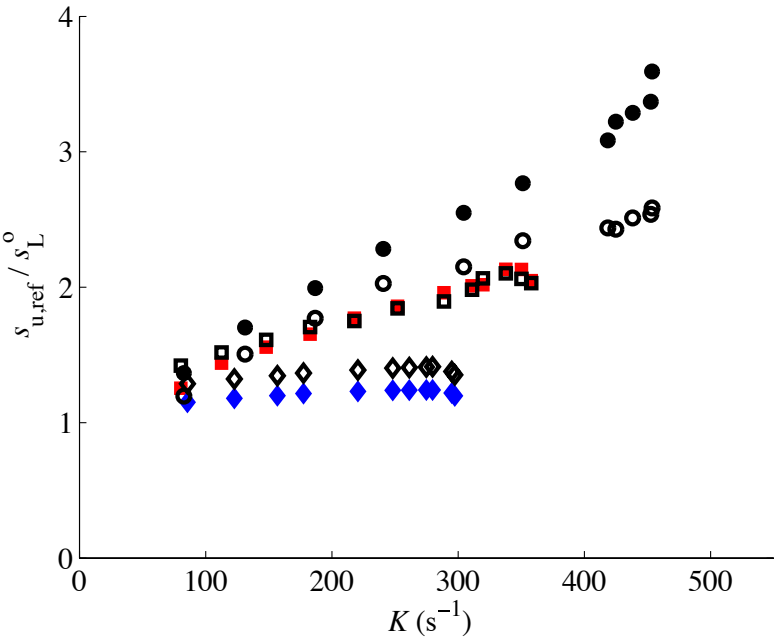

Figure 11: Experimental (solid symbols) and simulated (open symbols) reference stagnation flame speed versus stretch for premixed counter-flow flames: methane-air at $\phi = 0.6$ (■), propane-air at $\phi = 0.7$ (♦), hydrogen-air at $\phi = 0.19$ (●).

of $s_{\mathrm{u,ref}}$ measured for propane-air is underscored in Fig. 11 when compared to the larger increases in $s_{\mathrm{u,ref}}$ observed in methane-air and hydrogen-air cases.

Figure 7 showed modelled and experimental results for lean premixed laminar flames. Reference flame speed is extracted from modelled particle motion profiles by the same method used to measure experimental $s_{\mathrm{u,ref}}$: for methane and propane profiles, $s_{\mathrm{u,ref}}$ is the local minimum velocity upstream of the flame; for hydrogen-air, $s_{\mathrm{u,ref}}$ is the velocity at the point of the maximum in the profile's second derivative. Figure 11 shows the simulated

reference flame speeds together, normalized by their respective unstretched laminar flame speeds.

The performance of each mixture's chemical kinetic model is notably different. First, the presence of a maximum reference stagnation flame speed prior to extinction is predicted correctly for both methane-air and propane-air mixtures. Maximum stretched reference flame speeds from experiment and simulation are summarized in Table 2. Across all stretch rates for methane, in Fig. 11, simulations slightly over-predict $s_{\mathrm{u,ref}}$ at low K but the agreement between model and experiment improves with increasing stretch. This behaviour can partially be explained by the increasing correspondence between experimental flames and ideal one-dimensional flame assumptions as stretch increases [59]. GRI-Mech 3.0 is designed for premixed methane-air combustion and its ability correctly to predict the key features of these velocity profiles was anticipated.

To clarify the difference between model and experiment, Fig. 12 shows percent divergence in reference flame speed as a function of stretch rate for methane, propane and hydrogen. Positive values of divergence correspond to cases in which simulated $s_{\mathrm{u,ref}}$ is higher than the experimental measurement. Figure 12 includes uncertainty in the PTV measurement technique used to determine each $s_{\mathrm{u,ref}}$ value as a shaded uncertainty band plotted about the x-axis. Measurement uncertainty takes into account the systematic and random uncertainty at a 95% confidence interval. Systematic uncertainty in laser repetition rate is $\pm 0.1\%$ and pixel-to-length calibration coefficient is $\pm 0.8\%$. Uncertainty due to camera orientation and flow angle are negligible. Random error from the polynomial

	CH_4 + Air $\phi = 0.6$	C_3H_8 + Air $\phi = 0.7$	H_2 + Air $\phi = 0.19$
$s_{\mathrm{u,max-exp}}$	24.6 cm/s	24.4 cm/s	31.4 cm/s
$s_{\mathrm{u,max-sim}}$	24.3 cm/s	27.8 cm/s	22.6 cm/s

Table 2: Summary of maximum stretched flame speed from experiment and simulation.

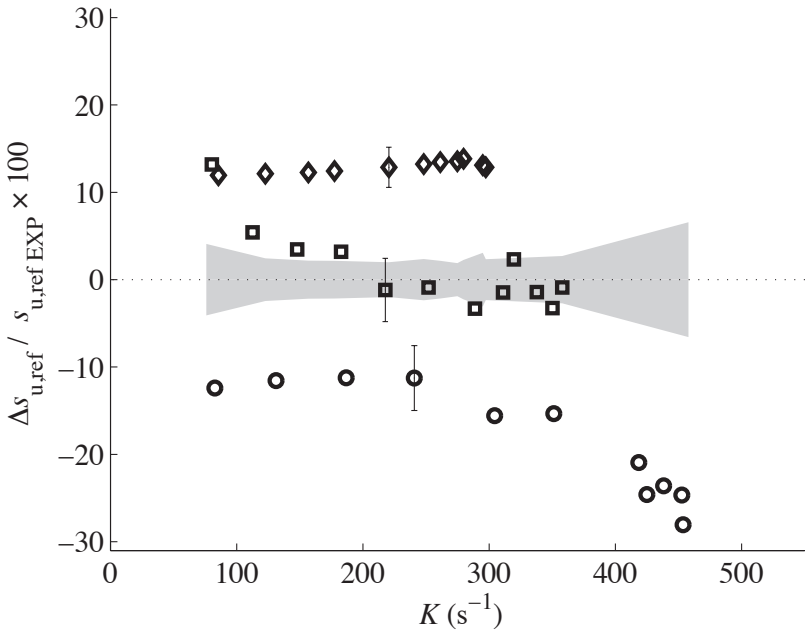

Figure 12: Divergence between model and experimental $s_{u,ref}$ with measurement uncertainty (shaded band) and experimental uncertainty (error bars): methane-air (□), propane-air (◇), hydrogen-air (○).

This is an

fit to the raw data is computed separately for each experimental run and is on the order of ±2.0%.

The uncertainty in simulated results due to measured boundary conditions is also shown in Fig. 12, where approximate uncertainty in atmospheric pressure is ±0.2%, inlet velocity is ±2.0% as above, inlet velocity gradient is ±4.7%, ambient temperature is ±0.3% and equivalence ratio is ±1.3%. These errors are propagated through the numerical model and reported as error bars for three cases [41, 57]. Figure 12 shows the divergence of methane-air simulations from experiment is on the order of the experimental uncertainty band across the range of conditions measured. Despite the increasingly one-dimensional behaviour of stretched flames, propane-air shows constant disagreement between model and experiment and hydrogen-air simulations diverge with increasing stretch (see Figs. 11 and 12).

In the case of propane-air, this nearly constant divergence, which Fig. 12 shows to be approximately 12%, indicates an error in the estimate of unstretched laminar flame speed used by the chemical kinetic mechanism, USC Mech II [36]. Extrapolating both experiment and model to zero stretch with the average delta between measurements reveals that USC Mech II over-predicts $s_{\mathrm{L}}^{\mathrm{o}}$ by 2.5 cm/s for the $\phi = 0.7$ case. In Fig. 13, the experimental results for propane-air are compared to USC Mech II simulations as well as the results of simulation with the C3 Davis-Law-Wang (DLW) mechanism [60]. The DLW mechanism is tuned for C1 to C3 hydrocarbons and contains 469 reactions and 71 species; it has been largely replaced by USC Mech II. Figure 13 shows that DLW gives good predictions of

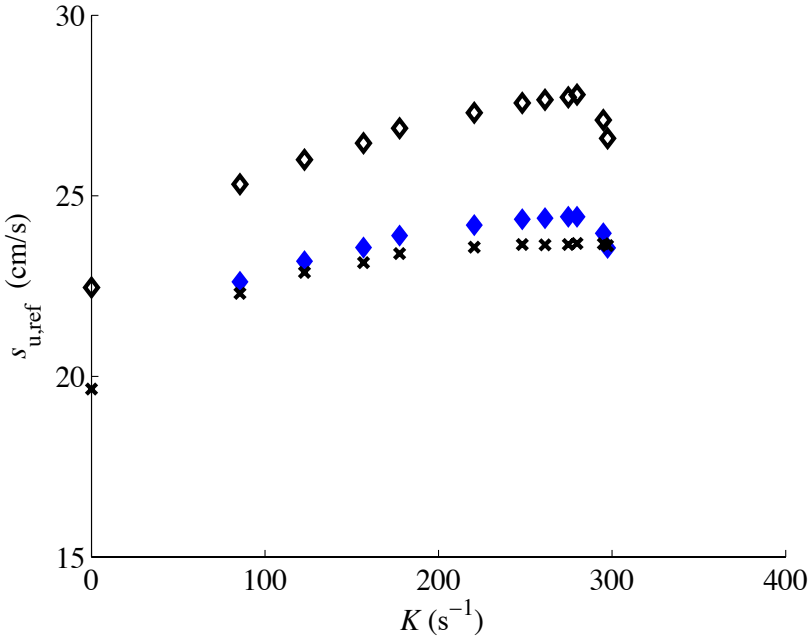

Figure 13: Comparison of experimental and modelled results for propane-air at $\phi = 0.7$: PTV results (⧫), USC Mech II (◇), DLW (×).

$s_{\mathrm{u,ref}}$, but that the trend near K_{ext} is not captured. While the agreement at lower K is superior in DLW, the ability of USC Mech II to capture the trend in $s_{\mathrm{u,ref}}$ near extinction indicates its ability to predict the kinetics for highly-stretched flames. The constant over-

prediction by USC Mech II can be improved by reducing the overall reactivity of propane-air at $\phi = 0.7$.

In the final case of hydrogen-air, Fig. 11 shows that while simulations predict the same increasing $s_{\mathrm{u,ref}}$ trend until extinction, experimental and predicted flame speeds appear to be diverging with increasing stretch. Increasing uncertainty in the PTV technique at high-stretch in the hydrogen cases is one possible explanation for this disparity, but the consistent deviation between model and experiment points to an overall modelled reactivity that is too low for these highly stretched, very lean hydrogen-air flames.

As Table 1 shows, the adiabatic flame temperatures in methane and hydrogen mixtures are comparatively low, relative to typical stoichiometric adiabatic flame temperatures on the order of 2000 K. The peak flame temperatures from CHEMKIN simulations are shown as a function of stretch rate in Fig. 14, where each point is taken from simulation, using the boundary conditions from a corresponding experimental run. Figure 14 demonstrates the preferential diffusion effect of increasing stretch on the flame's peak temperature. For

This is an

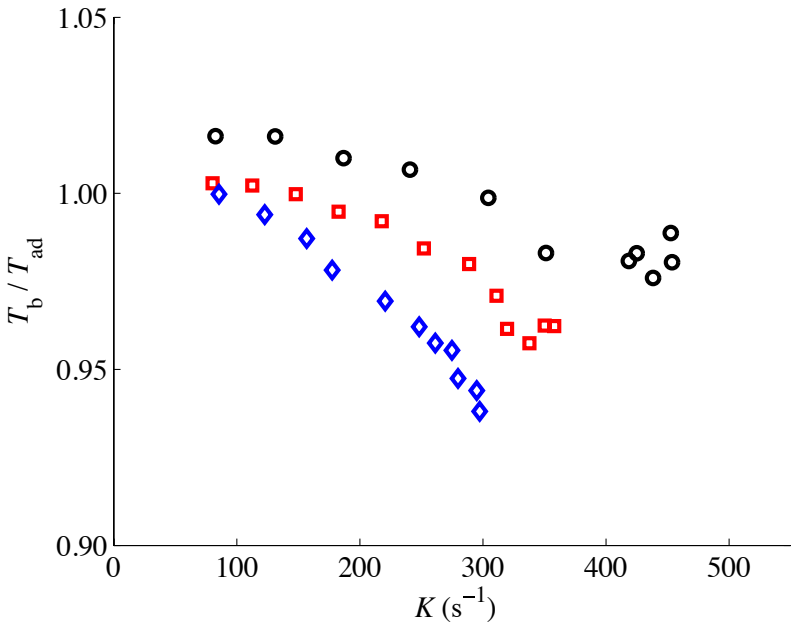

Figure 14: Normalized peak flame temperature, T_{b}, with stretch, K, for methane-air with $T_{\mathrm{ad}} = 1670\,\mathrm{K}$ (□), propane-air with $T_{\mathrm{ad}} = 1860\,\mathrm{K}$ (◇), hydrogen-air with $T_{\mathrm{ad}} = 1180\,\mathrm{K}$ (○).

Le $\gtrsim 1$ mixtures of methane and propane, flame temperature decreases with stretch. As the propane-air flame, with Le = 1.9, loses heat at a greater rate than it gains chemical energy, its flame temperature decreases at the highest rate and extinction occurs at the lowest K_{ext}. Alternatively, hydrogen-air with Le $\ll 1$ has a high centre-line flame temperature as its rate of chemical energy gain is greater than that of heat loss. At even the lowest stretch rates measured, hydrogen-air flames have T_{b} above T_{ad}. As stretch increases for this case, the reaction-zone is eventually constrained by the stagnation surface, flame temperature falls below the adiabatic flame temperature and extinction occurs by reduced residence time in the reaction zone. It should be noted that these simulated flame temperatures, obtained using boundary conditions directly measured in experiment, show temperature dependence on stretch that is different from the behaviour postulated in earlier works [1].

This is an

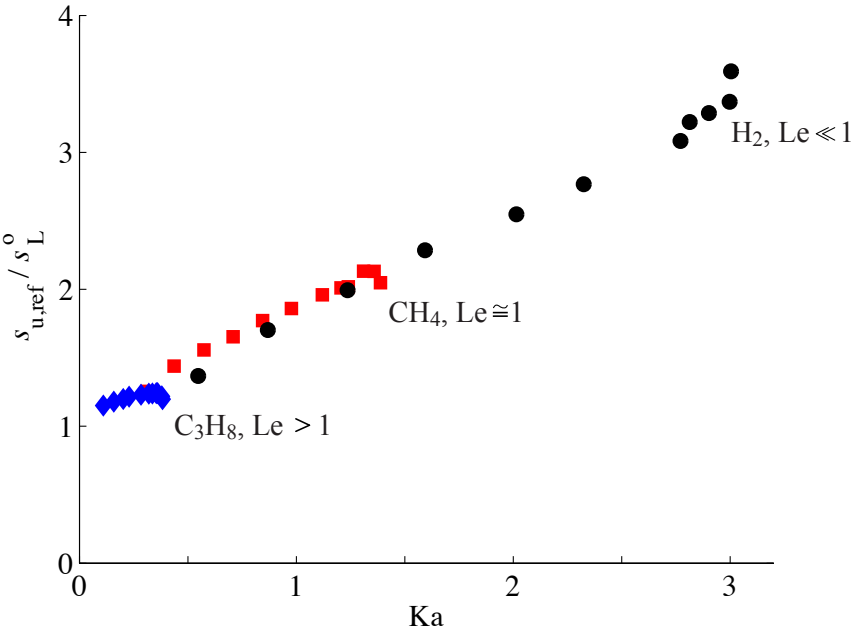

Figure 15: Experimental reference stagnation flame speed versus Karlovitz number for lean premixed counter-flow flames: methane-air at $\phi = 0.6$ (■), propane-air at $\phi = 0.7$ (♦), hydrogen-air at $\phi = 0.19$ (●).

In Fig. 15, non-dimensionalized reference flame speed is shown as a function of non-dimensionalized stretch. Reference flame speed is non-dimensionalized by $s_{\mathrm{L}}^{\mathrm{o}}$ as before, but now stretch rate is given as the Karlovitz number, Ka, defined as:

$$\mathrm{Ka} = K\frac{\delta_{\mathrm{L}}}{s_{\mathrm{L}}^{\mathrm{o}}} \ , \tag{9}$$

where δ_{L} is the laminar flame thickness. Figure 15 shows that the increase in reference flame speed appears to be linear with Ka, with similar slopes for all three flames, suggesting that reference flame speed depends primarily on stretch, flame thickness and laminar flame speed, but not on Lewis number.

In the above definition of the Karlovitz number, $\delta_{\mathrm{L}}/s_{\mathrm{L}}^{\mathrm{o}}$ represents the mixture's characteristic chemical reaction time and $1/K$ represents its characteristic flow time. For a diffusionally-balanced flame, extinction is expected to occur when these two characteristic times are of the same order [61]. Based on this interpretation of Karlovitz number, the results in Fig. 15 are a clear indication of preferential diffusion in fuel-lean methane, propane and hydrogen. For the diffusionally-balanced methane flames (Le $\cong$ 1), the $\mathrm{Ka}_{\mathrm{ext}}$ value is close to one since extinction occurs when the flow residence time becomes too short for complete reaction, as discussed above. In the case of the lean propane flame (Le $>$ 1), extinction is accelerated by the additional loss of heat through a diffusional imbalance in the flame, leading to the lower $\mathrm{Ka}_{\mathrm{ext}} = 0.35$. In contrast, for the lean hydrogen mixture (Le $\ll$ 1), the diffusional imbalance acts to strengthen the flame, preventing extinction until it is forced against the stagnation surface, with $\mathrm{Ka}_{\mathrm{ext}} = 3.0$. Table 3 summarizes the experimental results in the key figures: Figs. 10, 11 and 15.

5 Conclusions

This paper investigated the stretched, premixed, counter-flow combustion behaviour of mixtures with various preferential diffusion properties. While the behaviour of stretched

	CH_4 + Air $\phi = 0.6$	C_3H_8 + Air $\phi = 0.7$	H_2 + Air $\phi = 0.19$
K_{ext}	$358\,s^{-1}$	$297\,s^{-1}$	$454\,s^{-1}$
Ka_{ext}	1.39	0.354	3.00
$s_{u,max}$	24.6 cm/s	24.4 cm/s	31.4 cm/s
$s_{u,max}/s_L^o$	2.14	1.24	3.59

Table 3: Summary of stretched laminar flame experimental results.

flames is fairly well-understood, this study has experimentally verified some important aspects and clarified the key physics of these highly-stretched flames. Specifically, analysis of the results shows the following:

1. Experiments in stretched laminar flames have confirmed that $s_{u,ref}$ increases to a maximum at stretch rates below K_{ext} for Le $\gtrsim 1$ mixtures. For hydrogen-air with Le $\ll 1$, reaction rates increase with stretch and extinction only occurs by reduced residence time as a result of flow constraint against the stagnation surface.

This is an

2. The propane mixture has the highest s_L^o, but its flame is extinguished at a stretch rate of $K_{ext} = 297\,s^{-1}$ ($Ka_{ext} = 0.35$), with $s_{u,max}/s_L^o = 1.24$, the lowest of the three mixtures. This underscores the effect of preferential diffusion in Le > 1 mixtures, which lose heat through a diffusional imbalance in the flame and extinguish at lower stretch rate and Karlovitz number ($Ka_{ext} < 1$) due to a rapid decrease in reaction rates with increasing stretch.

3. Stretched laminar flame results show that hydrogen-air with $\phi = 0.19$ has a maximum stretched flame speed of $s_{u,max}/s_L^o = 3.6$ at the extinction stretch rate $K_{ext} = 454\,s^{-1}$ ($Ka_{ext} = 3.0$). The higher extinction stretch rate and Karlovitz number ($Ka_{ext} > 1$) is explained by the diffusional imbalance, which acts to strengthen the flame until it is constrained by the stagnation surface.

4. There is an apparent collapse of all mixtures' reference flame speeds when experimental results are plotted as a function of Karlovitz number as in Fig. 15. This

unexpected observation suggests the independence of $s_{u,ref}/s_L^o$ on Lewis number. In order to study this trend, further experiments are required in which Lewis number is varied independently of fuel composition.

Experimental results are also compared to numerical simulations performed using CHEMKIN. The chemical kinetics of methane and air are simulated by GRI-Mech 3.0, which performs well and agreement improves with stretch. USC Mech II is used to model propane and diverges from experiment by a constant amount across the range of stretch conditions, indicating a 12% error in the estimate of s_L^o for propane-air at $\phi = 0.7$. Lean hydrogen-air reactivity appears to be under-predicted by the Dryer H2-O2 mechanism with diverging predictions as stretch increases, but experimental uncertainty in the high-stretch results is relatively large and can partially explain this result. Most importantly, though, the models capture the important trends of a maximum in $s_{u,ref}$ ahead of the extinction stretch for methane and propane and an increasing $s_{u,ref}$ to extinction for hydrogen.

This is an

In summary, these experiments give clear indication of a maximum stretched reference flame speed before – or at – extinction for premixed flames. This maximum $s_{u,ref}$ depends on the Lewis number of the mixture. These findings can be applied to turbulent combustion experiments in order to examine the effect of a maximum stretched flame speed and extinction mechanisms for the same low, unity and high Lewis-number mixtures in premixed, turbulent counter-flow flames. Such experiments can reveal key turbulent flame propagation physics in the corrugated and thin reaction-zone regimes of premixed turbulent combustion.

Acknowledgments

The authors gratefully acknowledge the support of the Natural Sciences and Engineering Research Council of Canada and the Fonds Québécois de la Recherche sur la Nature et les Technologies. We also acknowledge the work of our colleague, P. Versailles, in developing the Particle Tracking Velocimetry technique employed.

References

[1] C. Law, Proceedings of the Combustion Institute 22 (1988) 1381–1402.

[2] F. Williams, Progress in Energy and Combustion Science 26 (2000) 657–682.

[3] R. W. Pitz, S. Hu, P. Wang, Progress in Energy and Combustion Science 42 (2014) 1–34.

[4] C. Law, Combustion Physics, Cambridge University Press, New York City, NY, 2006.

[5] G. Jackson, R. Sai, J. Plaia, C. Boggs, K. Kiger, Combustion and Flame 132 (2003) 503–511.

[6] G. Dixon-Lewis, Proceedings of the Royal Society of London Series A-Mathematical Physical and Engineering Sciences 462 (2006) 349–370.

[7] K. Kumar, C.-J. Sung, X. Hui, Fuel 90 (2011) 1004–1011.

[8] A. Cuoci, A. Frassoldati, T. Faravelli, E. Ranzi, Chemical Engineering Science 93 (2013) 266–276.

[9] L.-K. Tseng, M. Ismail, G. Faeth, Combustion and Flame 95 (1993) 410–426.

[10] S. Davis, J. Quinard, G. Searby, Combustion and Flame 130 (2002) 112–122.

This is an

[11] R. Johnston, J. Farrell, Proceedings of the Combustion Institute 30 (2005) 217–224.

[12] C. Tang, J. He, Z. Huang, C. Jin, J. Wang, X. Wang, H. Miao, International Journal of Hydrogen Energy 33 (2008) 7274–7285.

[13] E. Monteiro, M. Bellenoue, J. Sotton, N. A. Moreira, S. Malheiro, Fuel 89 (2010) 1985–1991.

[14] E. Varea, V. Modica, B. Renou, A. M. Boukhalfa, Proceedings of the Combustion Institute 34 (2013) 735–744.

[15] C. Law, International Journal of Heat and Mass Transfer 21 (1978) 1363–1368.

[16] J. Rolon, D. Veynante, J. Martin, F. Durst, Exp. Fluids 11 (1991) 313–324.

[17] L. Kostiuk, K. Bray, R. Cheng, Combustion and Flame 92 (1993) 396–409.

[18] E. Mastorakos, A. Taylor, J. Whitelaw, Combustion and Flame 102 (1995) 101–114.

[19] L. Kostiuk, I. Shepherd, K. Bray, Combustion and Flame 118 (1999) 129–139.

[20] D. Geyer, A. Kempf, A. Dreizler, J. Janicka, Combustion and Flame 143 (2005) 524–548.

[21] B. Böhm, D. Geyer, A. Dreizler, K. Venkatensan, N. Laurendeau, M. Renfro, Proceedings of the Combustion Institute 31 (2007) 709–717.

[22] K. Venkatesan, G. King, N. Laurendeau, M. Renfro, B. Böhm, Flow Turbulence and Combustion 83 (2009) 131–152.

[23] G. Coppola, A. Gomez, Experimental Thermal and Fluid Science 33 (2009) 1037–1048.

[24] G. Coppola, B. Coriton, A. Gomez, Physics of Fluids 22 (2010) 105101.

[25] V. Kuznetsov, V. Sabel'nikov, P. Libby (Eds.), Turbulence and Combustion, Hemisphere Publishing, Moscow, 1986.

[26] V. Karpov, A. Lipatnikov, V. Zimont, Flame curvature as a determinant of preferential diffusion effects in premixed turbulent combustion, in: W. Sirignano, A. Merzhanov, L. De Luca (Eds.), Advances in Combustion Science, AIAA, 1997, pp. 235–250.

[27] T.-W. Lee, G. North, D. Santavicca, Combustion and Flame 93 (1993) 445–456.

[28] A. Lipatnikov, J. Chomiak, Progress in Energy and Combustion Science 31 (2005) 1–73.

[29] P. Venkateswaran, A. Marshall, D. H. Shin, D. Noble, J. Seitzman, T. Lieuwen, Combustion and Flame 158 (2011) 1602–1614.

[30] P. Venkateswaran, A. Marshall, J. Seitzman, T. Lieuwen, Proceedings of the Combustion Institute 34 (2013) 1527–1535.

[31] B. Connelly, B. Bennett, M. Smooke, M. Long, Proceedings of the Combustion Institute 32 (2009) 879–886.

[32] F. N. Egolfopoulos, N. Hansen, Y. Ju, K. Kohse-Hoeinghaus, C. K. Law, F. Qi, Progress in Energy and Combustion Science 43 (2014) 36–67.

[33] J. Wehrmeyer, Z. Cheng, D. Mosbacher, R. Pitz, R. Osborne, Combustion and Flame 128 (2002) 232–241.

[34] L. Benezech, J. Bergthorson, P. Dimotakis, Proceedings of the Combustion Institute 32 (2009) 1301–1309.

[35] B. A. V. Bennett, C. S. McEnally, L. D. Pfefferle, M. D. Smooke, M. B. Colket, Combustion and Flame 156 (2009) 1289–1302.

[36] J. Bergthorson, S. Salusbury, P. Dimotakis, Journal of Fluid Mechanics 681 (2011) 340–369.

[37] B. A. Rankin, D. L. Blunck, V. R. Katta, S. D. Stouffer, J. P. Gore, Combustion and Flame 159 (2012) 2841 – 2843.

[38] L. Tosatto, F. Mella, M. B. Long, M. D. Smooke, Combustion and Flame 159 (2012) 3027–3039.

[39] G. A. Chung, B. Akih-Kumgeh, G. M. Watson, J. M. Bergthorson, Proceedings of the Combustion Institute 34 (2013) 831–838.

[40] G. M. G. Watson, J. D. Munzar, J. M. Bergthorson, Energy & Fuels 27 (2013) 7031–7043.

[41] G. M. G. Watson, J. D. Munzar, J. M. Bergthorson, Fuel 124 (2014) 113 – 124.

[42] B. Savard, G. Blanquart, Combustion and Flame 161 (2014) 1547–1557.

[43] K. Seshadri, F. Williams, International Journal of Heat and Mass Transfer 21 (1978) 251–253.

[44] M. Raffel, C. Willert, J. Kompenhans, Particle Image Velocimetry: A Practical Guide, Springer, 1998.

[45] J. Tien, M. Matalon, Combustion and Flame 84 (1991) 238–248.

[46] CHEMKIN-PRO rel. 15131, Reaction Design: San Diego (2014).

[47] G. Smith, D. Golden, M. Frenklach, N. Moriarty, B. Eiteneer, M. Goldenberg, C. Bowman, R. Hanson, S. Song, W. Gardiner, Jr., V. Lissianski, Z. Qin, `http://www.me.berkeley.edu/gri_mech/`, GRI-Mech 3.0 (1999).

[48] H. Wang, X. You, A. Joshi, S. Davis, A. Laskin, F. Egolfopoulos, C. Law, `http://ignis.usc.edu/USC_Mech_II.htm`, USC Mech Version II. High-Temperature Combustion Reaction Model of H2/CO/C1-C4 Compounds. (May 2007).

[49] M. Burke, M. Chaos, Y. Ju, F. Dryer, S. Klippenstein, International Journal of Chemical Kinetics 44 (2012) 444–474.

[50] R. Kee, J. Miller, G. Evans, G. Dixon-Lewis, Proceedings of the Combustion Institute 22 (1988) 1479–1494.

[51] J. Bergthorson, K. Sone, T. Mattner, P. Dimotakis, D. Goodwin, D. Meiron, Physical Review E 72.

[52] J. Bergthorson, D. Goodwin, P. Dimotakis, Proceedings of the Combustion Institute 30 (2005) 1637–1644.

[53] J. Bergthorson, P. Dimotakis, Proceedings of the Combustion Institute 31 (2007) 1139–1147.

[54] U. Niemann, K. Seshadri, F. A. Williams, Combustion and Flame 161 (2014) 138–146.

[55] C. Sung, C. Law, R. Axelbaum, Combustion Science and Technology 99 (1994) 119–132.

[56] C. Sung, C. Law, R. Axelbaum, Combustion and Flame 105 (1996) 189–201.

[57] J. Bergthorson, P. Dimotakis, Experiments in Fluids 41 (2006) 255–263.

[58] D. Goodwin, An open-source, extensible software suite for CVD process simulation., in: Proceedings of CVD XVI and EuroCVD Fourteen, Electrochemical Society, Paris, France, 2003, pp. 155–162.

[59] K. Sone, Modeling and simulation of axisymmetric stagnation flames, Ph.D. thesis, California Institude of Technology (2007).

[60] S. Davis, C. Law, H. Wang, Combustion and Flame 119 (1999) 375–399.

[61] N. Peters, Proceedings of the Combustion Institute 21 (1986) 1231–1250.

This is an